IEEE Access
Multidisciplinary | Rapid Review | Open Access Journal

Received May 9, 2019, accepted August 2, 2019, date of publication August 19, 2019, date of current version September 4, 2019.

Digital Object Identifier 10.1109/ACCESS.2019.2936224

Coupled Mode Analysis for 3D Stress-Free Elastic Acoustic Waveguide

JIAJI HE[1,2], (Student Member, IEEE), DANIEL HOMA[1,3], GARY PICKRELL[1,3], (Senior Member, IEEE), AND ANBO WANG[1,2], (Senior Member, IEEE)

[1]Center for Photonics Technology, Virginia Tech, Blacksburg, VA 24061, USA
[2]Department of Electrical and Computer Engineering, Virginia Tech, Blacksburg, VA 24061, USA
[3]Department of Material Science and Engineering, Virginia Tech, Blacksburg, VA 24060, USA

Corresponding author: Jiaji He (jiajihe@vt.edu)

This work was supported by the U.S. Department of Energy under Grant DE-NE0008665.

ABSTRACT Acoustic sensors and acoustic measurements receive much attention in various applications. Because waveguides are commonly used in sensor design, theoretical means to study acoustic propagation and interaction in waveguides are necessary. However, current methods for elastic wave coupling, including the transfer matrix method and coupled mode theory in planar 2D waveguides, are not satisfactory. In this work, a coupled mode analysis for acoustic waves in 3D stress-free elastic waveguides is proposed. Similar to the coupled mode theory in optical waveguides, the analysis is presented by the evolution of modal amplitudes. It can solve various modal conversion and scattering problems in elastic waveguides with small changes of cross sections and stress-free boundaries. To demonstrate the practicability, the coupled mode analysis is used to calculate the reflection spectrum of the newly proposed structure, the acoustic fiber Bragg grating. In a notch-based grating fabricated on a thin cylindrical waveguide, the results from coupled mode analysis are in good agreement with those from the transfer matrix method, which has been already validated experimentally. The coupled mode analysis is a promising method to solve various scattering problems.

INDEX TERMS Acoustic propagation, acoustic sensor, acoustic waves, Bragg gratings, coupled mode analysis.

I. INTRODUCTION

Sensing with acoustic waves is an important technology. By monitoring temperature [1]–[3], damage [4]–[6] and other parameters, an acoustic sensing system provides feedback controls for optimized operation and sends early warnings for potential failures. It could benefit multiple fields, such as aerospace [7], [8] and industrial plants [6], [9], [10].

A waveguide offers numerous advantages to a sensing system. The guided signal is easier to trace and has more defined signatures. Moreover, the waveguide could separate interrogation unit from hazardous environment. Therefore, waveguides are used in many sensing applications [1], [6], [9], [11]–[13]. Some sensing systems recognize environmental perturbations directly from the original waveguide through backscattered wave (including end reflections) [1], [11] and transmitted wave [12]. Other systems fabricate sensor structures in waveguides to enhance sensing ability. One such example is the recently proposed acoustic fiber Bragg grating (AFBG) [13], which introduces periodic variations of the cross sections of a waveguide.

Given the active applications of guided wave sensors, it is necessary to understand how acoustic modes interact with the waveguide and perturbations. Scattering from changed cross sections is of special interest, as it may be related to corrosion and crack initiation. A direct numerical finite element simulation could offer some results [14], [15], but analytical methods are desired to gain more insights. The transfer matrix method is a popular choice. It is shown capable of solving for axisymmetric [16]–[18] or non-axisymmetric cross sectional changes [17] in circular waveguides. However, the method is only developed for stepwise changes in cross sections. For continuously changing cross sections, the help of finite element simulation is usually needed [19].

In optical waveguides, coupled mode theory [20]–[22] is a widely used accurate tool to analyze modal conversion

The associate editor coordinating the review of this article and approving it for publication was Bora Onat.

in various applications of either continuous or stepwise waveguide perturbations, for example, optical fiber Bragg gratings (OFBGs) [23]. Considering the versatility of coupled mode theory and the similarities between optical waves and acoustic waves, it is natural to introduce a similar method to acoustic waves. Coupled mode analysis for pressure acoustic waves has been derived [24], [25]. For elastic media, some results were developed for waveguides in 2D Cartesian coordinates [26], [27] and extended into 2D curvilinear coordinates [28]. In these scenarios, the waveguide and modes have one-dimensional profiles. The waveguide is uniform in the other dimension, which is the propagation direction. In other words, the waveguide consists of planar or concentric circular layers. Hence, it is called 2D waveguide. 3D waveguides refer to those whose profiles or cross section must be described by two dimensions. Unfortunately, compared to the intense interest on 2D waveguides, treatment on 3D waveguide receives much less attention. Kennett introduced a 3D analysis [29], but the added dimension was another freedom of propagating direction. The waveguide had only one-dimensional profile and was still a 2D waveguide. Royer and Dieulesaint proposed another approach based on 3D waveguide [30], but it assumed vector fields can be expressed by a scalar and made an unrealistic oversimplification that only the density of waveguide material changed, while Lamé constants stayed the same. The results were of only qualitative meaning.

In this paper, a coupled mode analysis for 3D elastic waveguides is derived. The waveguide has stress-free boundaries. Perturbations to the waveguide are to change the outer shape of the cross section. From the assumption that perturbations are small, general coupled mode equations applicable for various waveguide perturbations are acquired, in the form of evolution of modal amplitudes along the propagation direction. As an example of application, explicit expressions are then derived with regards to AFBG in single mode region. To further determine the accuracy of the method, the results from coupled mode analysis are compared to existing experimentally-validated transfer matrix method in the special case of notch-AFBG, where the cross section has periodic step variations [13], [18]. Good agreement is found.

The paper is organized as follows: section II develops constraining equations of fields and mode orthogonality; section III derives the general coupled mode equations; section IV applies the theory to AFBG; section V compares the results of coupled mode theory and of transfer matrix method; section VI summarizes the work.

II. FIELD EQUATIONS AND MODE ORTHOGONALITY

Through the rest of the article, the term "unperturbed waveguide" will be used to refer to a waveguide with unchanged cross section. Modal profiles are acquired in an unperturbed waveguide. "Perturbed waveguide" means the cross section of the waveguide is changed slightly in shape near the boundary. The waveguide is formed by only solids and is placed in vacuum. Air-solid boundary is therefore not considered. Solid-vacuum boundary is stress-free.

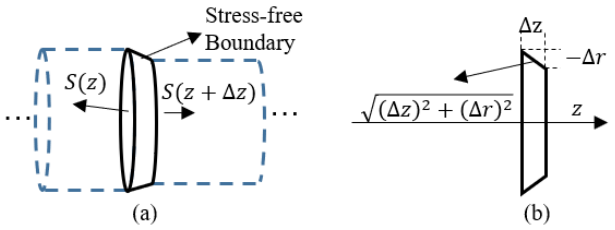

FIGURE 1. The slice of a perturbed waveguide with z as propagation axis. (a) A slice in the middle of waveguide is formed by two cross sections ($S(z)$, $S(z+\Delta z)$) and one boundary surface. (b) Related lengths are marked for $r(z+\Delta z) - r(z) = \Delta r < 0$ case.

The problem will be addressed in cylindrical coordinates. r_0 is the radius of unperturbed waveguide. z is the axis of waveguide and propagation. For ease of mathematical expression, the cross section of the unperturbed waveguide is circular and axisymmetric near its outer edges and the perturbation is also axisymmetric. As a result, the edges of cross section can be described by the radius $r(z)$. Note that unlike 2D waveguides, the assumption still allows for general non-axisymmetric structures inside the cross section, and it does not require the modal field to be axisymmetric at all. The analysis will be given in cylindrical coordinates. All fields are oscillating at angular frequency ω.

A. FIELD EQUATIONS FOR PERTURBED WAVEGUIDE

Displacement field $\boldsymbol{U}$ induces stress $\boldsymbol{T}$. $\boldsymbol{U}$ is a 3-element vector, and $\boldsymbol{T}$ is a 3-by-3 symmetric tensor. Suppose another displacement field $\boldsymbol{U}'$ induces $\boldsymbol{T}'$. In a sourceless medium, (1) applies for any closed surface.

$$0 = \int_{\text{all surface}} \mathrm{d}S \cdot \hat{\boldsymbol{n}} \cdot (\boldsymbol{T} \cdot \boldsymbol{U}' - \boldsymbol{T}' \cdot \boldsymbol{U}) \tag{1}$$

The relation is a variation from the reciprocity relation, namely (2.34) in [31], where by letting source term go zero and $\partial/\partial t = -j\omega$, the two volume integrals cancel out and only the surface integral remains. Apply (1) to a thin slice of perturbed waveguide as indicated in Figure 1.

The surface integral has two parts: integral on two cross sections; integral on the boundary surface. Let $\Delta z \to 0$. The first part can be expressed as a differential. Integral on $S(z)$ has negative sign because the surface normal is $-\hat{\boldsymbol{z}}$.

$$\begin{aligned}
&\left(\int_{S(z+\Delta z)} - \int_{S(z)}\right) \mathrm{d}S \cdot \hat{\boldsymbol{z}} \cdot (\boldsymbol{T} \cdot \boldsymbol{U}' - \boldsymbol{T}' \cdot \boldsymbol{U}) \\
&\quad \approx \Delta z \frac{\partial}{\partial z}\left[\int_{S(z)} \mathrm{d}S \cdot \hat{\boldsymbol{z}} \cdot (\boldsymbol{T} \cdot \boldsymbol{U}' - \boldsymbol{T}' \cdot \boldsymbol{U})\right] \\
&\quad = \Delta z \int_{S(z)} \mathrm{d}S \cdot \hat{\boldsymbol{z}} \cdot \frac{\partial}{\partial z}\left(\boldsymbol{T} \cdot \boldsymbol{U}' - \boldsymbol{T}' \cdot \boldsymbol{U}\right) \\
&\qquad + \Delta z \cdot r(z) \frac{\mathrm{d}r}{\mathrm{d}z} \int_0^{2\pi} \mathrm{d}\theta \cdot \hat{\boldsymbol{z}} \cdot \left(\boldsymbol{T} \cdot \boldsymbol{U}' - \boldsymbol{T}' \cdot \boldsymbol{U}\right)
\end{aligned} \tag{2}$$

For the second part, the surface normal is $\hat{\boldsymbol{n}} = (\Delta z \hat{\boldsymbol{r}} - \Delta r \hat{\boldsymbol{z}})/\sqrt{(\Delta z)^2 + (\Delta r)^2}$. Since $\Delta r/\Delta z \approx \mathrm{d}r/\mathrm{d}z$, the second

part changes into

$$\sqrt{(\Delta z)^2+(\Delta r)^2}\int_0^{2\pi} r\mathrm{d}\theta\cdot\hat{\boldsymbol{n}}\cdot\left(\boldsymbol{T}\cdot\boldsymbol{U'}-\boldsymbol{T'}\cdot\boldsymbol{U}\right) = \Delta z\int_0^{2\pi} r\mathrm{d}\theta\cdot\left(\hat{\boldsymbol{r}}-\frac{\mathrm{d}r}{\mathrm{d}z}\hat{\boldsymbol{z}}\right)\cdot\left(\boldsymbol{T}\cdot\boldsymbol{U'}-\boldsymbol{T'}\cdot\boldsymbol{U}\right). \quad (3)$$

The results in (2)(3) changes (1) into the form below.

$$0=\int_{S(z)}\mathrm{d}S\cdot\hat{\boldsymbol{z}}\cdot\frac{\partial}{\partial z}\left(\boldsymbol{T}\cdot\boldsymbol{U'}-\boldsymbol{T'}\cdot\boldsymbol{U}\right) + \int_0^{2\pi} r\mathrm{d}\theta\cdot\hat{\boldsymbol{r}}\cdot(\boldsymbol{T}\cdot\boldsymbol{U'}-\boldsymbol{T'}\cdot\boldsymbol{U})|_{r=r(z)} \quad (4)$$

Equation (4) is the equation for overall fields. The first term on right hand side corresponds to the coupling of fields along z. The second term is valued at the boundary $r(z)$. It indicates the impact of waveguide perturbation. The stress-free boundary condition for the perturbed waveguide is $0=\boldsymbol{T}\cdot\hat{\boldsymbol{n}}$, or explicitly

$$T_{rr}=\frac{\mathrm{d}r}{\mathrm{d}z}T_{rz},\quad T_{r\theta}=\frac{\mathrm{d}r}{\mathrm{d}z}T_{\theta z},\ T_{rz}=\frac{\mathrm{d}r}{\mathrm{d}z}T_{zz}\ \text{at}\ r(z). \quad (5)$$

This condition applies to the overall fields in the perturbed waveguide.

B. MODE ORTHOGONALITY RELATION

In an unperturbed waveguide, the fields of mode "m" are expressed as $\boldsymbol{U}_m=\boldsymbol{u}_m\exp(j\beta_m z-j\omega t)$ and $\boldsymbol{T}_m=\boldsymbol{t}_m\exp(j\beta_m z-j\omega t)$, where $\boldsymbol{u}_m,\boldsymbol{t}_m$ are mode profiles independent of z, and β_m is the propagation constant. The surface normal on boundary is now simply $\hat{\boldsymbol{r}}$. The stress-free boundary condition of mode "m" is

$$0=\boldsymbol{T_m}\cdot\hat{\boldsymbol{r}}\Leftrightarrow 0=T_{rrm}=T_{r\theta m}=T_{rzm}\quad \text{at}\ r=r_0. \quad (6)$$

In (4), set $\boldsymbol{U'},\boldsymbol{T'}=\boldsymbol{U}_n^*,\boldsymbol{T}_n^*$ and $\boldsymbol{U},\boldsymbol{T}=\boldsymbol{U}_m,\boldsymbol{T}_m$, where * means the complex conjugate. The unperturbed waveguide has $r(z)=r_0$ and $\mathrm{d}r/\mathrm{d}z=0$. Therefore, the second term on right hand side vanishes due to the boundary condition. For simplicity, it is assumed that no mode degeneracy is present. After a short derivation similar to [32], the mode orthogonality relation is reached.

$$j\delta_{mn}\frac{4}{\omega}P_m=\int_{S_0}\mathrm{d}S\cdot(u_{rn}^*t_{rzm}+u_{\theta n}^*t_{\theta zm}+u_{zn}^*t_{zzm} - u_{rm}t_{rzn}^*-u_{\theta m}t_{\theta zn}^*-u_{zm}t_{zzn}^*) \quad (7)$$

S_0 is the unperturbed cross section. δ_{mn} is the Kronecker delta. P_m is the power flow in $\hat{\boldsymbol{z}}$ direction carried by mode "m", calculated as

$$P_m=\frac{\omega}{2}\int_{S_0}\mathrm{d}S\cdot\Im\{u_{rm}^*t_{rzm}+u_{\theta m}^*t_{\theta zm}+u_{zm}^*t_{zzm}\}. \quad (8)$$

$\Im$ means taking imaginary part. If $P_m<0$, the power propagates in $-\hat{\boldsymbol{z}}$ direction.

III. COUPLED MODE EQUATION

The overall fields in a perturbed waveguide can be written as the superposition of modes in an unperturbed waveguide with evolving amplitudes, namely

$$\boldsymbol{U}=\sum_m a_m(z)\boldsymbol{U}_m=\sum_m a_m(z)\boldsymbol{u}_m e^{j\beta_m z-j\omega t}. \quad (9)$$

$\boldsymbol{T}$ is expanded in the same way. In (4), set $\boldsymbol{U'},\boldsymbol{T'}=\boldsymbol{U}_n^*,\boldsymbol{T}_n^*$ besides the expansion of $\boldsymbol{U},\boldsymbol{T}$, and it changes into

$$\begin{aligned}0=\sum_m\Bigg[&\left(j(\beta_m-\beta_n)a_m(z)+\frac{\mathrm{d}a_m(z)}{\mathrm{d}z}\right)e^{j(\beta_m-\beta_n)z}\\&\cdot\left(\int_{S(z)}\mathrm{d}S\cdot(u_{rn}^*t_{rzm}+u_{\theta n}^*t_{\theta zm}+u_{zn}^*t_{zzm})\right.\\&\left.-\int_{S(z)}\mathrm{d}S\cdot(u_{rm}t_{rzn}^*+u_{\theta m}t_{\theta zn}^*+u_{zm}t_{zzn}^*)\right)\Bigg]\\&+\int_0^{2\pi}r\mathrm{d}\theta(U_{rn}^*T_{rr}+U_{\theta n}^*T_{r\theta}+U_{zn}^*T_{rz})\\&-\int_0^{2\pi}r\mathrm{d}\theta(U_rT_{rrn}^*+U_\theta T_{r\theta n}^*+U_zT_{rzn}^*).\end{aligned} \quad (10)$$

and the last two integrals on the right side are valued at $r(z)$. Because $r(z)\approx r_0$, the boundary conditions of perturbed and unperturbed waveguides (5)(6) hold at the same time. Mode orthogonality relation (7) is applied to the summation term in (10) under $S(z)\approx S_0$ to simplify it into

$$j\frac{4}{\omega}P_n\frac{\mathrm{d}a_n(z)}{\mathrm{d}z} \quad (11)$$

The last integral term contains stress components of a single mode equaling zero from boundary condition (6). The second last integral term contains the overall stress in perturbed waveguide. Boundary condition (5) applies. That integral is rewritten as

$$\begin{aligned}&r_0\frac{\mathrm{d}r}{\mathrm{d}z}\int_0^{2\pi}\mathrm{d}\theta(U_{rn}^*T_{rz}+U_{\theta n}^*T_{\theta z}+U_{zn}^*T_{zz})\\&\quad=r_0\frac{\mathrm{d}r}{\mathrm{d}z}\sum_m a_m(z)e^{j\beta_m z-j\beta_n z}\int_0^{2\pi}\mathrm{d}\theta(u_{\theta n}^*t_{\theta zm}+u_{zn}^*t_{zzm}).\end{aligned} \quad (12)$$

$T_{rzm}=0$ from (6) is used as well. The simplification on all terms on the right-hand side of (10) leads to the explicit form below.

$$-P_n\frac{\mathrm{d}a_n(z)}{\mathrm{d}z}=\sum_m\kappa_{mn}a_m(z)e^{j\beta_m z-j\beta_n z} \quad (13)$$

where κ_{mn}, the coupling coefficient, is defined as

$$\kappa_{mn}=-j\frac{\omega}{4}r_0\frac{\mathrm{d}r}{\mathrm{d}z}\int_0^{2\pi}\mathrm{d}\theta(u_{\theta n}^*t_{\theta zm}+u_{zn}^*t_{zzm})_{r=r_0}. \quad (14)$$

Equation (13) is the general form of coupled mode analysis for acoustic waves in perturbed elastic waveguides. Solving (13) for all modes concerned leads to the evolution of the overall fields. In many cases, (13) has an analytic solution. Otherwise, many well-developed ordinary differential equation solver can conveniently acquire a numerical solution.

It is obvious that (13) has a similar form as the coupled mode theory for optical waveguides, for example (2) in [21].

IV. APPLICATION ON SINGLE-MODE WEAK AFBG

Like the OFBG concept, an AFBG is a periodic structure in an acoustic waveguide that reflects elastic wave of matched wavelength [13]. The word "weak" means the perturbation of the AFBG structure is small. Suppose the AFBG has period Λ. When the central wavenumber of AFBG $\beta_c = \pi/\Lambda$ equals the propagation constant of wave β, the AFBG has strongest reflection. This is the phase matching condition.

For simplicity, the waveguide operates in single mode region, where only forward propagating fundamental mode "1" with $\beta_1 = \beta$ and backward mode "-1" with $\beta_{-1} = -\beta$ are considered. Set $\Delta\beta = \beta_1 - \beta_{-1} = 2\beta$. Define detuning δ as $1 + \delta = \beta/\beta_c$. Then $r(z)$ and coupling coefficient κ_{mn} can be expanded into Fourier series.

$$r = r_0 + \sum_{p=-\infty}^{+\infty} \Delta r_p \cdot e^{j2p\beta_c z} \tag{15}$$

$$\kappa_{mn} = \kappa_{mn}^{(0)} \beta_c \left(\sum_{p=-\infty}^{+\infty} p\Delta r_p \cdot e^{j2p\beta_c z} \right) \tag{16}$$

with

$$\kappa_{mn}^{(0)} = \frac{\omega}{2} r_0 \int_0^{2\pi} \mathrm{d}\theta (u_{\theta n}^* t_{\theta zm} + u_{zn}^* t_{zzm})_{r=r_0}. \tag{17}$$

Let $n = 1$, $m = 1, -1$, and expand (13).

$$-P_1 \frac{\mathrm{d}a_1(z)}{\mathrm{d}z} = \sum_p \kappa_{-1,1}^{(0)} p\beta_c \Delta r_p \cdot a_{-1}(z) e^{2j(p-1-\delta)\beta_c z} + \sum_p \kappa_{1,1}^{(0)} p\beta_c \Delta r_p \cdot a_1(z) e^{j2p\beta_c z} \tag{18}$$

Waves close to the phase matching condition are of interest, so consider only $|\delta| \ll 1$. In an OFBG, only the term with the smallest exponent is dominant. Under the "synchoronous approximation" [23], [33], the rest terms have rapidly oscillating z dependence and are neglected. Following the same argument, here all terms on the right side can be neglected, except for $\kappa_{-1,1}^{(0)} \beta_c \Delta r_1 a_{-1}(z) \exp(-2j\delta\beta_c z)$ ($p = 1$ in the first term). The same phase-matching approximation can also be applied to $n = -1$ case in (13). The simplified coupled mode equations for the AFBG is shown below.

$$P_1 \frac{\mathrm{d}a_1(z)}{\mathrm{d}z} = -\kappa_{-1,1}^{(0)} \beta_c \Delta r_1 \cdot a_{-1}(z) e^{-2j\delta\beta_c z} \tag{19}$$

$$P_{-1} \frac{\mathrm{d}a_{-1}(z)}{\mathrm{d}z} = \kappa_{1,-1}^{(0)} \beta_c \Delta r_{-1} \cdot a_1(z) e^{2j\delta\beta_c z} \tag{20}$$

The mode profile of backward "-1" mode can be expressed as the complex conjugate of "1" mode, i.e. $\boldsymbol{u}_{-1} = \boldsymbol{u}_1^*, \boldsymbol{t}_{-1} = \boldsymbol{t}_1^*$. This leads to $P_1 = -P_{-1} > 0$ and $\kappa_{1,-1}^{(0)} = (\kappa_{-1,1}^{(0)})^*$. Assume the AFBG starts at $z = 0$ and ends at $z = L$. For boundary conditions of the ordinary differential equations (19)(20), $a_1(0)$ is the known input. $a_{-1} = 0$ because no coupling happens afterwards. Then, in the AFBG region,

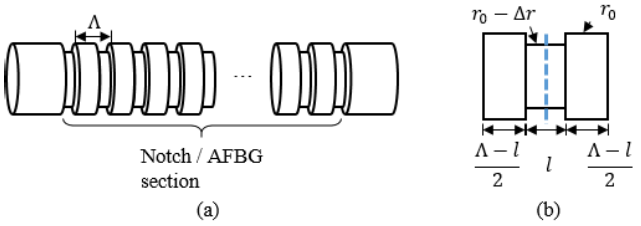

FIGURE 2. Periodic notches. (a), the schematic; (b), a single node used in transfer matrix method.

(19)(20) are easily solved as shown below.

$$a_1(z) = a_1(0) \frac{j\delta\beta_c \sinh\xi(z-L) + \xi\cosh\xi(z-L)}{-j\delta\beta_c \sinh\xi L + \xi\cosh\xi L} e^{-j\delta\beta_c z} \tag{21}$$

$$a_{-1}(z) = -a_1(0) \frac{\kappa_{1,-1}^{(0)} \beta_c \Delta r_{-1}}{P_1} \frac{\sinh\xi(z-L)}{-j\delta\beta_c \sinh\xi L + \xi\cosh\xi L} e^{j\delta\beta_c z} \tag{22}$$

The symbol ξ stands for

$$\xi = \beta_c \sqrt{-\delta^2 + \frac{1}{P_1^2} |\kappa_{1,-1}^{(0)}|^2 \Delta r_1 \Delta r_{-1}}. \tag{23}$$

The reflection coefficient, defined as the ratio of amplitudes at input $a_{-1}(0)/a_1(0)$, can then be calculated.

$$R_{coupled} = \frac{\kappa_{1,-1}^{(0)} \Delta r_{-1}}{P_1} \frac{\beta_c \sinh\xi L}{-j\delta\beta_c \sinh\xi L + \xi\cosh\xi L} \tag{24}$$

V. COMPARISON TO TRANSFER MATRIX METHOD IN NOTCH-AFBG

Notch-AFBG is fabricated by engraving periodic circular notches around a thin cylindrical rod. Transfer matrix method can be used to calculate the reflection spectrum [13], [18], [34]–[36]. The method breaks down the AFBG into repeated cascading nodes. It then derives the transfer matrix of a single node and therefore the overall transfer matrix of the entire AFBG. The notch-AFBG and the nodes are shown in Figure 2. The notches have period Λ, notch length l and cut depth $\Delta r > 0$ (radius at notch is $r_0 - \Delta r$).

Transfer matrix method was experimentally validated with good accuracy [13]. In this section, it serves as a reference for the coupled mode analysis.

It should be mentioned that in this section, the expressions from coupled mode analysis is reduced to a 2D form only because it is in need to compare its accuracy with known theoretical and experimental results in 2D structures. The results of AFBG derived from coupled mode analysis in Section IV applies to general 3D structures and to non-axisymmetric modes.

A. MODAL FIELD EXPRESSIONS

The waveguide outside the AFBG region is a stress-free infinitely long thin cylindrical rod. The waveguide operates

in single-mode region with the lowest longitudinal mode L_{01}. Its displacement field has only r and z components.

$$u_r = k_{tl}AJ_1(k_{tl}r) - j\beta CJ_1(k_{ts}r) \tag{25}$$
$$u_z = -j\beta AJ_0(k_{tl}r) + k_{ts}CJ_0(k_{ts}r) \tag{26}$$

with $k_{tl} = \sqrt{\omega^2/V_l^2 - \beta^2}$, $k_{ts} = \sqrt{\omega^2/V_s^2 - \beta^2}$. V_l and V_s are longitudinal and shear wave speed respectively. Coefficients A, C are linked by boundary conditions. To simplify the expression, asymptotic form $J_0(x) \approx 1$ and $J_1(x) \approx x/2$ are used because the arguments of Bessel functions $(k_{tl}r, k_{ts}r)$ are small in a thin rod. Furthermore, J_1 terms are relatively small compared to J_0. Hence, u_r can be neglected and u_z simplified as

$$u_z = -j\beta A + k_{ts}C. \tag{27}$$

The same approximation can be used to approximate stress components.

$$t_{rr} = t_{\theta\theta} = j\lambda\beta u_z \tag{28}$$
$$t_{zz} = j(\lambda + 2\mu)\beta u_z \tag{29}$$

λ, μ are Lamé constants. The rest components are zero. Note that $\boldsymbol{u}$ and $\boldsymbol{t}$ are actual fields without the phase factor $\exp(j\beta z - j\omega t)$. The fields are uniform across the cross section, provided the waveguide is thin.

The simplified stress-free boundary condition leads to $-2jA\beta k_{tl}^2 + C(k_{ts}^2 - \beta^2)k_{ts} = 0$ [30]. In forward propagating "1" mode, set C to be real. Then jA, u_{z1} are real. $t_{rr1}, t_{\theta\theta 1}, t_{zz1}$ are purely imaginary. Therefore,

$$\boldsymbol{u}_{-1} = \boldsymbol{u}_1^* = \boldsymbol{u}_1, \quad \boldsymbol{t}_{-1} = \boldsymbol{t}_1^* = -\boldsymbol{t}_1. \tag{30}$$

B. RESULTS FROM COUPLED MODE ANALYSIS

To apply coupled mode analysis, assume the first node of the AFBG starts at $z = 0$ and the last (N-th) node ends at $z = N\Lambda$ and the notch is shallow or $\Delta r \ll r_0$. In the AFBG region, the radius profile is a periodic rectangular pulse.

$$r(z) = \begin{cases} r_0 - \Delta r, \\ \quad \left(p + \frac{1}{2}\right)\Lambda - \frac{1}{2}l \le z < \left(p + \frac{1}{2}\right)\Lambda + \frac{1}{2}l \\ r_0, \quad \text{elsewhere} \end{cases} \tag{31}$$

p is a natural number. The profile can be decomposed into Fourier series.

$$r(z) = r_0 - \Delta r\frac{l}{\Lambda} - \sum_{p=1}^{+\infty}\frac{2\Delta r}{p\pi}(-1)^p \sin(p\beta_c l)\cos(2p\beta_c z) \tag{32}$$

The results in Section IV can be directly used with

$$\Delta r_1 = \Delta r_{-1} = \frac{\Delta r}{\pi}\sin(\pi\frac{l}{\Lambda}). \tag{33}$$

Note that $\beta_c = \pi/\Lambda$. Take (27)-(30) into (8)(17) to get

$$P_1 = \frac{\omega}{2}\pi r_0^2 \Im\{u_{z1}^* t_{zz1}\} = \frac{\omega}{2}\pi r_0^2(\lambda + 2\mu)\beta_1 u_{z1}^2 \tag{34}$$

$$\kappa_{1,-1}^{(0)} = \pi\omega r_0 u_{z1} t_{zz1} = j\pi\omega r_0(\lambda + 2\mu)\beta_1 u_{z1}^2 \tag{35}$$
$$\kappa_{-1,1}^{(0)} = (\kappa_{1,-1}^{(0)})^* = -j\pi\omega r_0(\lambda + 2\mu)\beta_1 u_{z1}^2 \tag{36}$$

Combine the result above with (23)(24) to get reflection coefficient from coupled mode theory. $L = N\Lambda$.

$$R_{coupled} = -\frac{2\Delta r_1}{r_0}\frac{\sinh N\pi\frac{\xi}{\beta_c}}{\delta\sinh N\pi\frac{\xi}{\beta_c} + j\frac{\xi}{\beta_c}\cosh N\pi\frac{\xi}{\beta_c}} \tag{37}$$

$$\xi = \beta_c\sqrt{-\delta^2 + \frac{4\Delta r_1^2}{r_0^2}} \tag{38}$$

C. RESULTS FROM TRANSFER MATRIX METHOD

The transfer matrix of a single node can be solved following the steps indicated in [13].

$$M = \begin{pmatrix} \alpha_1 & \alpha_2 \\ \alpha_3 & \alpha_4 \end{pmatrix},$$

where

$$\alpha_1 = \alpha_4^* = e^{j\beta(\Lambda - l)}[\cos\beta l + j\frac{1/\gamma + \gamma}{2}\sin\beta l] \tag{39}$$
$$\alpha_2 = -\alpha_3 = j\frac{\gamma - 1/\gamma}{2}\sin\beta l \tag{40}$$

$\gamma = (r_0 - \Delta r)^2/r_0^2$ is the ratio of cross sectional area. The overall transfer matrix M^N of N nodes is the multiplication of each individual matrix.

$$M^N = \frac{\lambda_2\lambda_1^N - \lambda_1\lambda_2^N}{\lambda_2 - \lambda_1}I + \frac{\lambda_2^N - \lambda_1^N}{\lambda_2 - \lambda_1}T_i \tag{41}$$
$$\lambda_1 = \frac{1}{2}\left[\alpha_1 + \alpha_4 + \sqrt{4\alpha_2\alpha_3 + (\alpha_1 - \alpha_4)^2}\right] \tag{42}$$
$$\lambda_2 = \frac{1}{2}\left[\alpha_1 + \alpha_4 - \sqrt{4\alpha_2\alpha_3 + (\alpha_1 - \alpha_4)^2}\right] \tag{43}$$

and the reflection coefficient is

$$R_{mat} = -(M^N)_{21}/(M^N)_{22} = 2\left[\frac{\alpha_1 - \alpha_4}{\alpha_3} + \frac{\lambda_1^N + \lambda_2^N}{\lambda_2^N - \lambda_1^N}\sqrt{-4 + \left(\frac{\alpha_1 - \alpha_4}{\alpha_3}\right)^2}\right]^{-1} \tag{44}$$

This is the form of the exact transfer matrix method for a thin rod. To compare it with the coupled mode theory and to simplify the complicated expression, the notch is again assumed to be small i.e. $\Delta r/r_0 \ll 1$. This leads to $\gamma \approx 1 - 2\Delta r/r_0$ and $1/\gamma \approx 1 + 2\Delta r/r_0$. The following simplified forms are then reached.

$$\lambda_1 = -\cos\delta\pi + \sqrt{\frac{4\Delta r^2}{r_0^2}\sin^2(1 + \delta)\pi\frac{l}{\Lambda} - \sin^2\delta\pi} \tag{45}$$

$$\lambda_2 = -\cos\delta\pi - \sqrt{\frac{4\Delta r^2}{r_0^2}\sin^2(1 + \delta)\pi\frac{l}{\Lambda} - \sin^2\delta\pi} \tag{46}$$

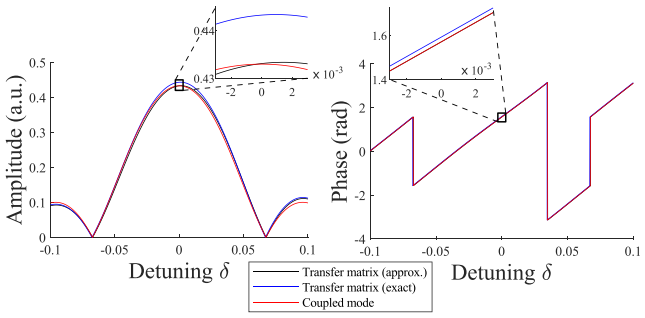

FIGURE 3. Reflection spectra from both methods. "Coupled mode" is from (37); "Transfer matrix (exact)" is from (44); "Transfer matrix (approx.)" is from (47). The insets are a enlarged version around the phase-matching point. (a) the amplitude of reflection coefficient R. Relative difference at $\delta = 0$ is 2.1%. (b) the phase of R. The constant π jump means sign inversion of amplitude.

$$R'_{mat} = \frac{-\frac{2\Delta r}{r_0}\sin(1+\delta)\pi\frac{l}{\Lambda}}{\sin\delta\pi + j\frac{\lambda_1^N+\lambda_2^N}{\lambda_2^N-\lambda_1^N}\sqrt{\frac{4\Delta r^2}{r_0^2}\sin^2(1+\delta)\pi\frac{l}{\Lambda} - \sin^2\delta\pi}} \tag{47}$$

Equation (37) will be denoted as the reflection coefficient of approximated transfer matrix method.

In [13], an alternative narrow-notch approximation (assuming $l \ll \Lambda$ in addition to shallow notch) to (44) is derived in its appendix from (16) to (27). It should be pointed out that this approximation is incorrect, as it gives reflection coefficient $|R| \propto N$ under perfect phase-matching condition $\delta = 0$, meaning $|R|$ can go to infinity, whereas in reality, $|R| \leq 1$. The mistake originates from claiming $\alpha_2\alpha_3 \approx 0$ in (15) in its appendix ((42)(43) in this article), while at $\delta = 0$, $|\alpha_2\alpha_3| \gg (\alpha_1 - \alpha_4)^2 \approx 0$. Yet despite the obvious error, Figure 2 in [13] shows the narrow notch result agrees well with the exact form. To further understand the apparent contradiction, a deeper study into the narrow-notch approximation, with details omitted in this article, is performed. It concludes that the approximation only fails around a very narrow region near $\delta = 0$ (almost as narrow as a point) and maintains good agreement to the exact form elsewhere. It might happen that no sampling point falls into the failure region, so the two results seem to overlap well in the plot. Nevertheless, excluding only the $\delta = 0$ point, the exact form matches well with the narrow-notch approximation shown in Figure 2 in [13]; the approximation also agrees with experimental measurements shown in in Figure 5(b) in [13]. Hence, it can still be concluded that experimental data validates the exact form of transfer matrix method. It will still be used as a reference for comparison below. It should be pointed out that results in (37)(44)(47) here in this article do not assume narrow notches.

D. COMPARISON BETWEEN TWO METHODS

First, the reflection spectrum of an AFBG with $l = 0.1\Lambda$, $\Delta r = 0.05r_0$, and $N = 20$, is calculated by both methods and shown in Figure 3.

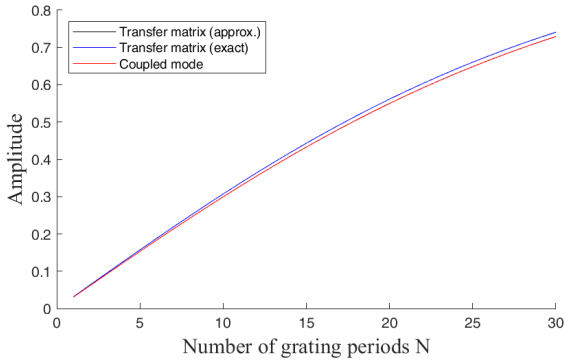

FIGURE 4. Amplitude of reflection coefficient ($|R|$) at phase-matching point ($\delta = 0$) in AFBGs of varying length. $l = 0.1\Lambda$, $\Delta r = 0.05r_0$. Red line of coupled mode analysis and black line from approximated transfer matrix are almost overlapping so black line is not clearly seen.

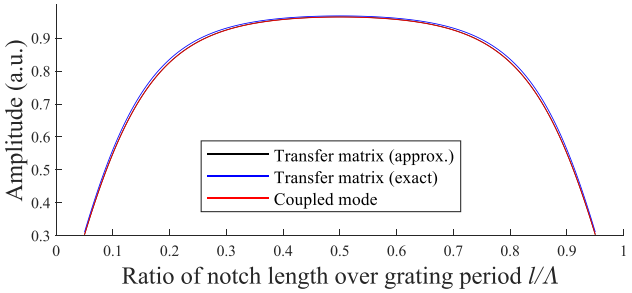

FIGURE 5. Amplitude of reflection coefficient ($|R|$) at phase-matching point ($\delta = 0$) in AFBGs of varying notch length. $N = 20$, $\Delta r = 0.05r_0$. Red line of coupled mode analysis and black line from approximated transfer matrix are almost overlapping so black line is not clearly seen.

It can be seen that the coupled mode analysis and the approximated transfer matrix method have very close results. The lines almost overlap. Although discrepancy is present with regards to the exact transfer matrix method, the relative difference is only 2.1% around $\delta = 0$.

Second, the reflection coefficients at the phase-matching point ($\delta = 0$) are calculated for AFBGs of varying length with $l = 0.1\Lambda$, $\Delta r = 0.05r_0$. The results are shown in Figure 4.

A similar conclusion could be drawn. Approximated transfer matrix method and coupled mode analysis have close results. Their differences from the exact transfer matrix method are less than 3.9%. The maximum relative difference appears at $N = 1$ and then gradually reduces as N increases. It is 1.6% at $N = 30$.

Third, the length of each notch is set to vary but $N = 20$, $\Delta r = 0.05r_0$ are fixed. The results are shown in Figure 5.

Within the plotted region ($0.05 < l/\Lambda < 0.95$), coupled mode analysis almost overlaps with the approximated transfer matrix method. Their relative differences from the exact transfer matrix method are less than 2.5%.

Fourth, consider an infinite grating, or $N \to \infty$. At $\delta = 0$, it can be easily derived that $R_{coupled} = j$. For the approximated transfer matrix method, $|\lambda_1| < 1 \Rightarrow \lambda_1^N = 0$. This leads to $R'_{mat} = j = R_{coupled}$. Both methods fit the anticipation that an infinite periodic structure will totally reflect incident waves that satisfy the Bragg condition

(wavelength $= 2\Lambda$). The exact transfer matrix method does not have a simple solution under $N \to \infty$ and $\delta = 0$.

From all four comparisons, it is concluded that in this notch-AFBG application, the coupled mode theory is as precise as the transfer matrix method under the shallow notch approximation, and very close to the exact method. Since the transfer matrix method is validated through experiments [13], the coupled mode analysis is validated as well.

Although the exact transfer matrix method has better accuracy in this application, its use is limited. First, the expression is so complicated that it is normally presented numerically. A direct physical understanding is not easy to acquire. Second, reported applications are strongly limited to L_{01} mode in thin waveguides [18], [34]–[36], where the mode has plane-wave profile. Last, the method requires the change of cross section to be stepwise. The approximated transfer matrix method does not have the first disadvantage, but still has the rest two, while its precision is no longer better. On the contrary, the coupled mode analysis has none of these limitations. It can work with any modes after the coupling coefficients and modal power are calculated from the modal profiles at no cost of lowered precision. It can be applied to any stress-free waveguides with changing cross sections with a good accuracy, provided the perturbation is small.

VI. CONCLUSION

In this article, a coupled mode analysis is proposed. It solves mode coupling and wave scattering problems by calculating the evolution of modal amplitudes. The analysis applies to waveguides with changing cross sections and stress-free boundaries. The form derived generally applies to most stress-free waveguides, with the only limitation that the waveguide must only be slightly changed. As an example of its application, it is used to calculate the reflection spectrum of the newly proposed AFBG structure. An explicit and relatively simple form is obtained. A further comparison to the existing experimentally verified transfer matrix method is performed on a notch-based AFBG with $l = 0.1\Lambda$, $\Delta r = 0.05r_0$. The results from the coupled mode analysis matches well with the transfer matrix method under shallow notch approximation, and is less than 2.7% away from the exact transfer matrix solution. With validated accuracy and little limitation, the coupled mode analysis offers a powerful tool in solving various wave propagation problems.

ACKNOWLEDGMENT

The authors would like to thank Mr. Zachary Hileman, Mr. Steven Snider, and Miss Ruixuan Wang for their kind discussion on this work, as well as Dr. Di Hu and Dr. Haifeng Xuan for the help on improving the transfer matrix method.

REFERENCES

[1] N. Gopalsami and A. C. Raptis, "Acoustic velocity and attenuation measurements in thin rods with application to temperature profiling in coal gasification systems," *IEEE Trans. Sonics Ultrason.*, vol. SU-31, no. 1, pp. 32–39, Jan. 1984.

[2] C. E. Weld, J. D. Sternhagen, R. D. Mileham, K. D. Mitzner, and D. W. Galipeau, "Temperature measurement using surface skimming bulk waves," in *Proc. IEEE Int. Ultrason. Symp.*, vol. 1, Oct. 1999, pp. 441–444.

[3] P. Shakkottai and S. P. Venkateshan, "System for temperature profile measurement in large furnances and kilns and method therefor," U.S. Patent 4 762 425, Aug. 9, 1988.

[4] C. Jen, Z. Sun, and M. Kobayashi, "Ultrasonic monitoring of barrel wear and screw status," in *Proc. Antec Conf.*, vol. 1, 2004, pp. 402–406.

[5] H. Tattersall, "The ultrasonic pulse-echo technique as applied to adhesion testing," *J. Phys. D, Appl. Phys.*, vol. 6, no. 7, p. 819, 1973.

[6] D. Alleyne, B. Pavlakovic, M. Lowe, and P. Cawley, "Rapid, long range inspection of chemical plant pipework using guided waves," in *Proc. AIP Conf.*, vol. 557, 2001, pp. 180–187.

[7] V. Giurgiutiu, J. M. Redmond, D. P. Roach, and K. Rackow, "Active sensors for health monitoring of aging aerospace structures," *Proc. SPIE*, vol. 3985, pp. 294–306, Jun. 2000.

[8] W. G. Schwarz, M. E. Read, M. J. Kremer, M. K. Hinders, and B. T. Smith, "Lamb wave tomographic imaging system for aircraft structural health assessment," *Proc. SPIE*, vol. 3586, pp. 292–297, Jan. 1999.

[9] J. L. Rose, J. J. Ditri, A. Pilarski, K. Rajana, and F. Carr, "A guided wave inspection technique for nuclear steam generator tubing," *NDT E Int.*, vol. 27, no. 6, pp. 307–310, 1994.

[10] M. G. Silk and K. F. Bainton, "The propagation in metal tubing of ultrasonic wave modes equivalent to Lamb waves," *Ultrasonics*, vol. 17, no. 1, pp. 11–19, 1979.

[11] C.-K. Jen, J.-G. Legoux, and L. Parent, "Experimental evaluation of clad metallic buffer rods for high temperature ultrasonic measurements," *NDT E Int.*, vol. 33, no. 3, pp. 145–153, 2000.

[12] C. H. Wang, J. T. Rose, and F.-K. Chang, "Computerized time-reversal method for structural health monitoring," *Proc. SPIE*, vol. 5046, pp. 48–59, Aug. 2003.

[13] D. Hu, H. Xuan, Z. Yu, D. Y. Wang, B. Liu, J. He, and A. Wang, "Acoustic fiber Bragg grating and its application in high temperature sensing," *IEEE Sensors J*, vol. 18, no. 23, pp. 9576–9583, Dec. 2018.

[14] R. Carandente, J. Ma, and P. Cawley, "The scattering of the fundamental torsional mode from axi-symmetric defects with varying depth profile in pipes," *J. Acoust. Soc. Amer.*, vol. 127, no. 6, pp. 3440–3448, Jun. 2010.

[15] M. J. S. Lowe, D. N. Alleyne, and P. Cawley, "The mode conversion of a guided wave by a part-circumferential notch in a pipe," *J. Appl. Mech.*, vol. 65, no. 3, pp. 649–656, 1998.

[16] H. E. Engan, "Torsional wave scattering from a diameter step in a rod," *J. Acoust. Soc. Amer.*, vol. 104, no. 4, pp. 2015–2024, 1998.

[17] J. J. Ditri, "Utilization of guided elastic waves for the characterization of circumferential cracks in hollow cylinders," *J. Acoust. Soc. Amer.*, vol. 96, no. 6, pp. 3769–3775, 1994.

[18] A. Morales, J. Flores, L. Gutiérrez, and R. A. Méndez-Sánchez, "Compressional and torsional wave amplitudes in rods with periodic structures," *J. Acoust. Soc. Amer.*, vol. 112, no. 5, pp. 1961–1967, 2002.
[19] R. Kirby, Z. Zlatev, and P. Mudge, "On the scattering of longitudinal elastic waves from axisymmetric defects in coated pipes," *J. Sound Vib.*, vol. 332, no. 20, pp. 5040–5058, 2013.
[20] A. W. Snyder, "Coupled-mode theory for optical fibers," *J. Opt. Soc. Amer.*, vol. 62, no. 11, pp. 1267–1277, Nov. 1972.
[21] A. Yariv, "Coupled-mode theory for guided-wave optics," *IEEE J. Quantum Electron.*, vol. QE-9, no. 9, pp. 919–933, Sep. 1973.
[22] H. Haus and W. P. Huang, "Coupled-mode theory," *Proc. IEEE*, vol. 79, no. 10, pp. 1505–1518, Oct. 1991.
[23] T. Erdogan, "Fiber grating spectra," *J. Lightw. Technol.*, vol. 15, no. 8, pp. 1277–1294, Aug. 1997.
[24] R. B. Evans, "A coupled mode solution for acoustic propagation in a waveguide with stepwise depth variations of a penetrable bottom," *J. Acoust. Soc. Amer.*, vol. 74, no. 1, pp. 188–195, 1983.
[25] J. A. Fawcett, "A derivation of the differential equations of coupled-mode propagation," *J. Acoust. Soc. Amer.*, vol. 92, no. 1, pp. 290–295, 1992.
[26] V. Maupin, "Surface waves across 2-D structures: A method based on coupled local modes," *Geophys. J. Int.*, vol. 93, no. 1, pp. 173–185, 1988.
[27] V. Pagneux and A. Maurel, "Lamb wave propagation in elastic waveguides with variable thickness," *Proc. Roy. Soc. A, Math., Phys. Eng. Sci.*, vol. 462, no. 2068, pp. 1315–1339, 2006.
[28] V. Galanenko, "On coupled modes theory of two-dimensional wave motion in elastic waveguides with slowly varying parameters in curvilinear orthogonal coordinates," *J. Acoust. Soc. Amer.*, vol. 103, no. 4, pp. 1752–1762, 1998.
[29] B. L. N. Kennett, "Guided wave propagation in laterally varying media—I. Theoretical development," *Geophys. J. Int.*, vol. 79, no. 1, pp. 235–255, 1984.
[30] D. Royer and E. Dieulesaint, *Elastic Waves in Solids I: Free and Guided Propagation*, D. P. Morgan, Ed. New York, NY, USA: Springer-Verlag, 2000.
[31] K. Aki and P. Richards, *Quantitative Seismology, Theory and Methods*, vol. 1. San Francisco, CA, USA: W. H. Freeman, 1980.
[32] J. J. Ditri and J. L. Rose, "Excitation of guided elastic wave modes in hollow cylinders by applied surface tractions," *J. Appl. Phys*, vol. 72, no. 7, pp. 2589–2597, 1992.
[33] H. Kogelnik, "Theory of optical waveguides," in *Guided-Wave Optoelectronics*. Berlin, Germany: Springer, 1988, pp. 7–88.
[34] D. Li and H. Benaroya, "Waves, normal modes and frequencies in periodic and near-periodic rods. Part II," *Wave Motion*, vol. 20, no. 4, pp. 339–358, 1994.
[35] B. Ravindra, "Love-theoretical analysis of periodic system of rods," *J. Acoust. Soc. Amer.*, vol. 106, no. 2, pp. 1183–1186, 1999.
[36] D. J. Griffiths and C. A. Steinke, "Waves in locally periodic media," *Amer. J. Phys*, vol. 69, no. 2, pp. 137–154, 2001.

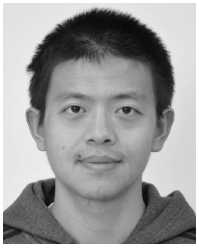

JIAJI HE received the B.S. degree in electronic engineering from Tsinghua University, Beijing, China, in 2014. He is currently pursuing the Ph.D. degree in electrical engineering with Virginia Polytechnic Institute and State University (Virginia Tech, a.k.a.), Blacksburg, VA, USA, where he has been a Graduate Research Assistant with the Center for Photonics Technology, since 2014.

His research interest includes fiber sensors and acoustic sensors.

DANIEL HOMA received the B.S., M.S., and Ph.D. degrees from Rutgers University. He is currently an Associate Research Professor with the Department of Material Science and Engineering, Virginia Tech, Blacksburg, VA, USA.

GARY PICKRELL received the B.S. and M.S. degrees from Ohio State University and the Ph.D. degree from Virginia Tech, Blacksburg, VA, where he is currently a Professor with the Department of Material Science and Engineering.

He is the Rolls Royce Commonwealth Director of Surface Engineering, the Director of Nano-Bio Materials Laboratory, and an Associate Director of the Center for Photonics Technology. He is the author of over 200 publications, including 17 Books, 16 patents, and three special journal issues, more than 90 Journals, and 90 conference papers.

ANBO WANG received the Ph.D. degree in optics from the Dalian University of Technology, China, in 1990. He is currently the Clayton Ayre Professor with the Bradley Department of Electrical and Computer Engineering, Virginia Tech, Blacksburg, VA, where he is also the Director of the Center for Photonics Technology. His research interests include optical sensors and their applications.